Supplementary Information for:

Formation of colour centres in lead-iodide perovskites: Self-trapping and defects in bulk and surfaces

Francesco Ambrosio,[a,b,*] Edoardo Mosconi,[b] Ahmed A. Alasmari,[c,d] Fatmah A. S. Alasmary,[e] Daniele Meggiolaro,[b] Filippo De Angelis [a,b,e,f*]

[a]*CompuNet, Istituto Italiano di Tecnologia, Via Morego 30, 16163 Genova, Italy.*

[b]*Computational Laboratory for Hybrid/Organic Photovoltaics (CLHYO), Istituto CNR di Scienze e Tecnologie Chimiche "Giulio Natta" (CNR-SCITEC), Via Elce di Sotto 8, 06123 Perugia, Italy.*

[c]*The First Industrial Institute, TVTC, Riyadh, Saudi Arabia.*

[d]*Physics and Astronomy Department, College of Science, King Saud University, Riyadh, Saudi Arabia.*

[e]*Chemistry Department, College of Science, King Saud University, Riyadh, Saudi Arabia.*

[f]*Department of Chemistry, Biology and Biotechnology, University of Perugia, Via Elce di Sotto 8, 06123 Perugia, Italy.*

*E-mail: Francesco.Ambrosio@iit.it, filippo@thch.unipg.it

S1. Models of $MAPbI_3$

For bulk tetragonal $MAPbI_3$, we employ a 384-atoms 2×2×2 supercell with lattice parameters $a = b$ = 17.72 Å, c = 25.32 Å, corresponding to the experimental structure.[1] The employed model correspond the most stable structure of tetragonal $CH_3NH_3PbI_3$ at 0 K and reasonably represents the system at low temperature, but above the phase transition to the orthorhombic phase.[2] In this model, MA cations are arranged in such a way that no net dipole is present in the system.[2] The results achieved with this computational setup have been benchmarked against calculations performed on larger supercells.[2] For the bulk orthorhombic phase (o-$MAPbI_3$), we consider a 2×1×2 192-atoms supercell with lattice parameters a = 17.81, b = 12.82 Å, c = 17.32 Å. Calculations of the surface of tetragonal $MAPbI_3$ are performed on different models of the (001) surface of tetragonal $CH_3NH_3PbI_3$: (i) a 408-atoms slab terminated with lead diiodide (PbI_2) (cf. Fig. S1, left panel), (ii) a 552-atoms slab terminated with methylammonium iodide (MAI), (cf. Fig. S1, right panel), and (iii) a slab with 50% MAI coverage. For all the systems, the simulation cell has $a = b$ = 17.70 Å, c = 50 Å, with the latter including a vacuum layer of 20 (25) Å for MAI (PbI_2) slab, a computational setup that has been benchmarked in previous studies.[3] We focus on the (001) surface since both theoretical calculations[4, 5] and X-ray diffraction experiments[6] indicate that this is one of the dominant facets in tetragonal $MAPbI_3$. We note that the arrangement of MA cations in the slab model is such that the direction of the molecular dipoles is alternated (cf. the MA molecules along the x direction in Fig. S1), thus implying that that the net dipole field is minimal along the z direction. Furthermore, for electronic-structure calculations involving slab models, the electrostatic potential is corrected by compensating for the surface dipole, as implemented in CP2K following Ref. 7.

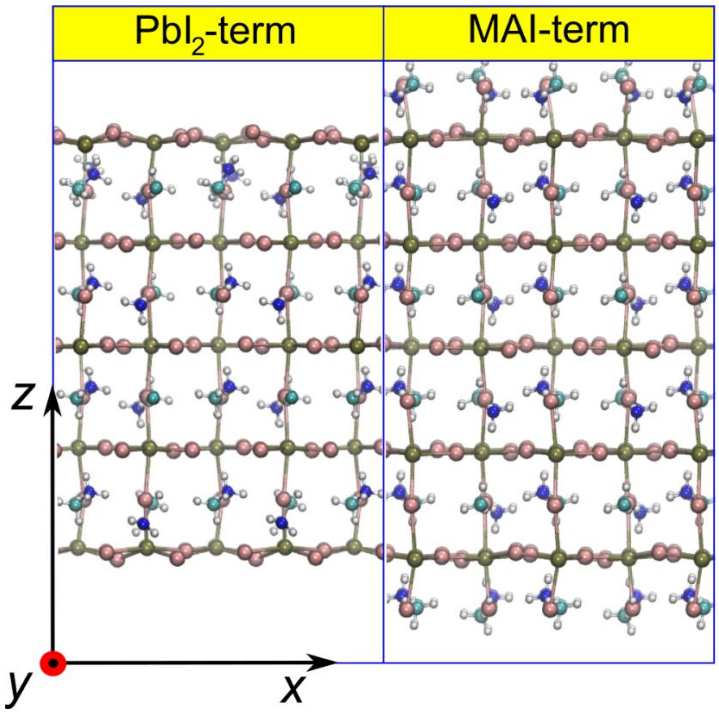

Figure S1. Stick&ball representation of the PbI_2 and MAI (001) surfaces of tetragonal $MAPbI_3$. Lead in brown, iodine in pink, nitrogen in blue, carbon in cyan, and hydrogen in white.

S2. Effect of slab thickness on the electronic properties

The 5-layers slab employed to model the (001) $MAPbI_3$ surface has been tested in previous work. It has been noted that the position of the band edges is quite stable with respect to slab thickness.[8] This implies that the energetics of defects, which is influenced by the position of band edges, is not affected by slab thickness.[8] Furthermore, it was found that charge localization and the energetics of polarons are unaffected by the thickness of the slab, when using slabs with 6 and 7 PbI_2 layers. [9] To further assess the validity of our model, we calculate $\Delta E(\mathrm{IFD})$ (cf. main text for definition) for the PbI_2-terminated slabs with 6 and 7 PbI_2 layers. The calculated values, collected in Table S1, show differences below 0.1 with respect to the one using the 5-layers slab are below 0.1 eV. Furthermore, analysis of the wave-function for the models with 6 and 7 layers indicates that hole localization is essentially unaffected by the thickness of the slab (cf. Fig. S2). We also report the respective electronic density of states (DOS), cf. Fig. S3.

Table S1. Calculated values of $\Delta E(\mathrm{IFD})$ (eV, cf. main text for definition) for bulk tetragonal $MAPbI_3$ for PbI_2-terminated slabs with different number of layers.

Layers	$\Delta E(\mathbf{IFD})$
5	-0.85
6	-0.88
7	-0.90

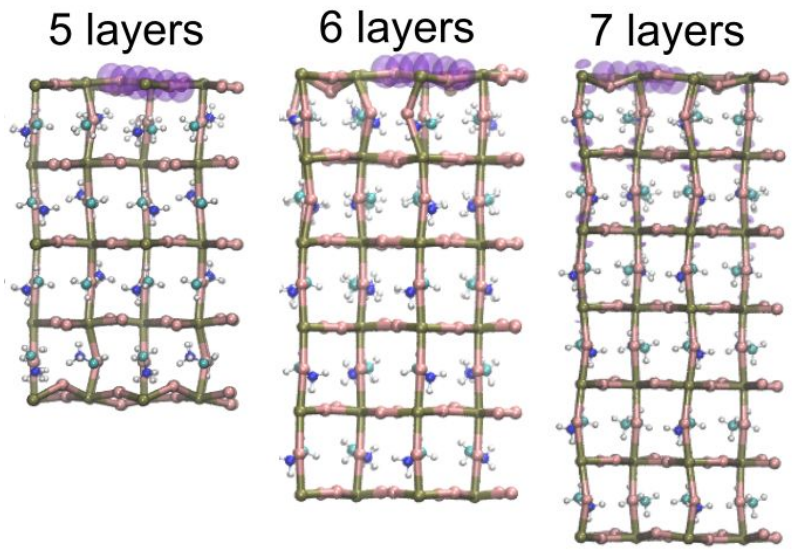

Figure S2. Isodensity representations of the hole captured by the IFD on the (001) PbI_2 terminated surface of tetragonal $MAPbI_3$ for slabs with different number of layers.

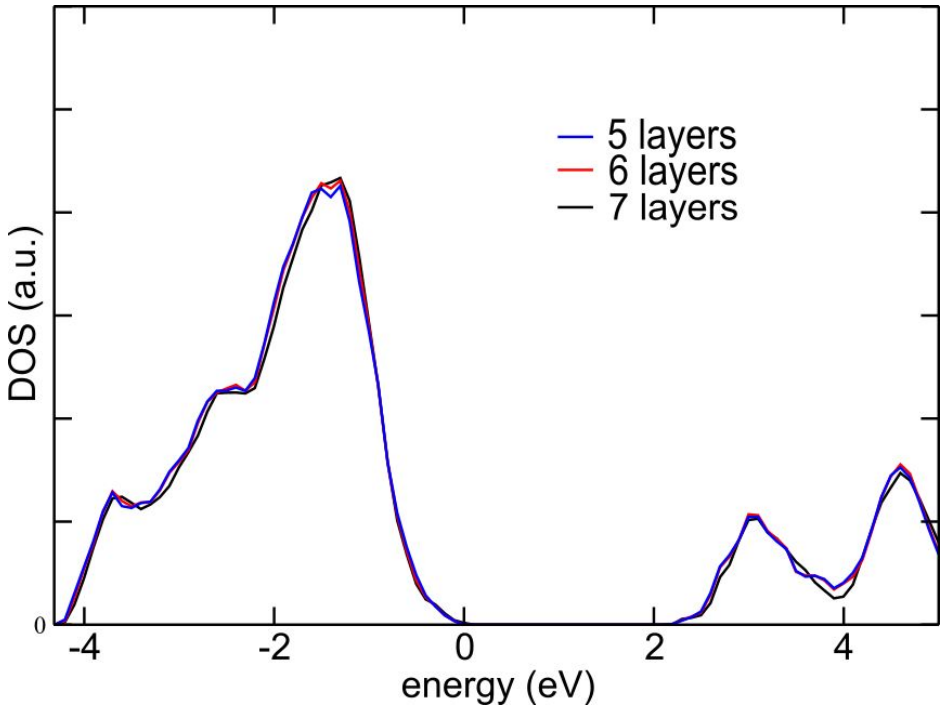

Figure S3. Electronic density of states (DOS) of the valence and conduction band states for the IFD on the (001) PbI_2 terminated surface of tetragonal $MAPbI_3$ for slabs with different number of layers. The energies are referred to the valence band edge of the 5-layer slab and are aligned through core levels.

S3. Energetics of the V-center in o-$MAPbI_3$ at different levels of theory

We here calculate $\Delta E(V_k^+)$ (cf. main text) for o-$MAPbI_3$ at different levels of theory. In order to be fully consistent with the results reported in Ref. 10, all calculations are carried out with VASP[11] using 400 eV energy cut-off and DFT-D3[12, 13] dispersion interactions. We perform geometry optimization of o-$MAPbI_3$ in presence of an extra hole with and without the I_2^- dimer at (i) the DFT+U[14, 15] levels with different values of the the Hubbard-like term U and (ii) at the hybrid functional level of theory employing both the PBE0 and HSE06[16, 17] hybrid functionals, in which the fraction of Fock exchange α is set to 0.188 [referred as PBE0(α) and HSE06(α) in Table S2] following Ref. 10. Furthermore, we perform extra calculations in which we include spin-orbit coupling through fully relativistic pseudopotentials by (i) reevaluating the wave-function for the structures achieved without SOC

(labelled as "sp" in Table S1) and (ii) carrying out geometry optimization at the HSE06(α)+SOC level. Finally, we also consider the effect of *k*-point sampling, using a 1×2×1 mesh.

Table S2. Values of $\Delta E(\mathrm{V})$ (cf. main text) for the 2×1×2 supercell of o-$MAPbI_3$ as achieved at different levels of theory.

	Theoretical Level	$\Delta E(\mathrm{V_k^+})$
2×1×2 at Γ	DFT+U (8.9)	-0.19
	DFT+U (6.7)	-0.04
	DFT+U (4.5)	-0.13
	HSE06(α)	0.28
	HSE06(α)+SOC(sp)	0.27
	HSE06(α)+SOC	0.39
	PBE0(α)	0.32
	PBE0(α)+SOC(sp)	0.31
2×1×2 K121	HSE06(α)	0.39
	HSE06(α)+SOC(sp)	0.47
	HSE06(α)+SOC	0.46

We first note that results achieved at the DFT+U level of theory are sizably influenced by the value of the Hubbard-like term. While for a value of $\mathrm{U} = 8.9$ eV we reproduce the results of Ref. 10 ($\Delta E(\mathrm{V}) = -0.19$ eV), we observe that the relative stability of the systems with and without the dimer varies with U. In particular, at $\mathrm{U} = 4.5$ eV, the system bearing the dimer is found to be less stable by 0.14 eV. In contrast, calculations performed with PBE0(α) and HSE06(α), provide a consistent physical picture, in which the dimer is found always at higher energies with values of $\Delta E(\mathrm{V}) = 0.32$ and 0.28 eV, respectively. The effect of SOC is moderate, a consequence of the mild impact of SOC on the energetics of valence band states. Results achieved with *k*-point sampling seem to favor even more

the semi-localized hole over the dimer, with an effect of ~0.1 eV. Overall, our in-depth analysis demonstrates that self-trapping of holes on I_2^- dimers should not be expected in o-$MAPbI_3$.

S4. Energetics of IFDs for $MAPbI_3$ (bulk and surfaces)

Table S3. Calculated values of $\Delta E(\mathrm{IFD})$ (cf. main text) for bulk tetragonal $MAPbI_3$ and for different termination of the (001) surface. All values are given in eV.

System	$\Delta E(\mathbf{IFD})$
Bulk	0.24
MAI-terminated	0.32
50% MAI-terminated	– 0.24
PbI_2-terminated	– 0.85

S5. Representation of the IFD in tetragonal bulk $MAPbI_3$

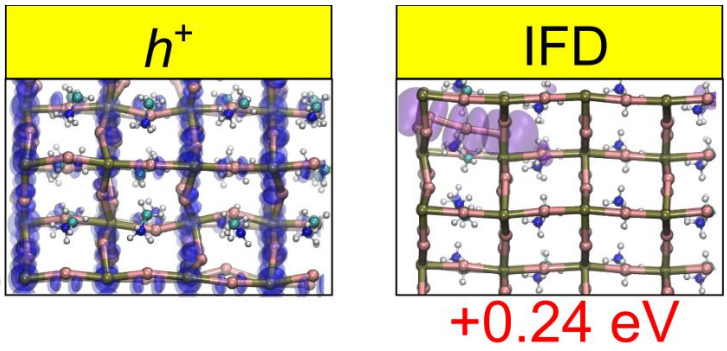

Figure S4. Schematic representation of the energetics associated with trapping of a two in bulk tetragonal $MAPbI_3$. Pb atoms are given in brown, I in pink, C in cyan, N in blue, and H in white. The isodensity representation of the hole is given as shaded purple for each system. The tetragonal axis lies horizontally.

S6. Representation of the IFD on the 50% MAI-covered (001) surface of $MAPbI_3$

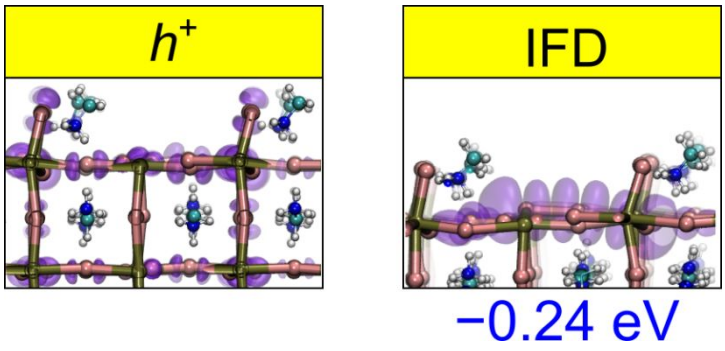

Figure S5. Schematic representation of the energetics associated with trapping of a two holes on the 50% MAI-covered (001) surface of $MAPbI_3$. Pb atoms are given in brown, I in pink, C in cyan, N in blue, and H in white. The isodensity representation of the hole is given as shaded purple for each system. A side view with the *z* axis of the slab lying vertically is represented in the all the figures.

References

1. Kawamura, Y.; Mashiyama, H.; Hasebe, K., Structural Study on Cubic–Tetragonal Transition of $CH_3NH_3PbI_3$. *J. Phys. Soc. Jpn* **2002,** *71* (7), 1694-1697.

2. Quarti, C.; Mosconi, E.; De Angelis, F., Interplay of Orientational Order and Electronic Structure in Methylammonium Lead Iodide: Implications for Solar Cell Operation. *Chem. Mater.* **2014,** *26* (22), 6557-6569.

3. Meggiolaro, D.; Mosconi, E.; De Angelis, F., Formation of Surface Defects Dominates Ion Migration in Lead-Halide Perovskites. *ACS Energy Lett.* **2019,** *4* (3), 779-785.

4. Haruyama, J.; Sodeyama, K.; Han, L.; Tateyama, Y., Termination Dependence of Tetragonal $CH_3NH_3PbI_3$ Surfaces for Perovskite Solar Cells. *J. Phys. Chem. Lett.* **2014,** *5* (16), 2903-2909.

5. Haruyama, J.; Sodeyama, K.; Han, L.; Tateyama, Y., Surface Properties of $CH_3NH_3PbI_3$ for Perovskite Solar Cells. *Acc. Chem. Res.* **2016,** *49* (3), 554-561.

6. Baikie, T.; Fang, Y.; Kadro, J. M.; Schreyer, M.; Wei, F.; Mhaisalkar, S. G.; Graetzel, M.; White, T. J., Synthesis and Crystal Chemistry of the Hybrid Perovskite $(CH_3NH_3)PbI_3$ for Solid-State Sensitised Solar Cell Applications. *J. Mater. Chem. A* **2013,** *1* (18), 5628-5641.

7. Bengtsson, L., Dipole Correction for Surface Supercell Calculations. *Phys. Rev. B* **1999,** *59* (19), 12301-12304.

8. Meggiolaro, D.; Mosconi, E.; Proppe, A. H.; Quintero-Bermudez, R.; Kelley, S. O.; Sargent, E. H.; De Angelis, F., Energy Level Tuning at the $MAPbI_3$ Perovskite/Contact Interface Using Chemical Treatment. *ACS Energy Lett.* **2019,** *4* (9), 2181-2184.

9. Ambrosio, F.; Meggiolaro, D.; Mosconi, E.; De Angelis, F., Charge Localization and Trapping at Surfaces in Lead-Iodide Perovskites: The Role of Polarons and Defects. *J. Mater. Chem. A* **2020,** *8* (14), 6882-6892.

10. Peng, C.; Wang, J.; Wang, H.; Hu, P., Unique Trapped Dimer State of the Photogenerated Hole in Hybrid Orthorhombic $CH_3NH_3PbI_3$ Perovskite: Identification, Origin, and Implications. *Nano Lett.* **2017,** *17* (12), 7724-7730.

11. Kresse, G.; Furthmüller, J., Efficiency of Ab-Initio Total Energy Calculations for Metals and Semiconductors Using a Plane-Wave Basis Set. *Comput. Mater. Sci.* **1996,** *6* (1), 15-50.

12. Grimme, S.; Ehrlich, S.; Goerigk, L., Effect of the damping Function in Dispersion Corrected Density Functional Theory. *J. Comput. Chem.* **2011,** *32* (7), 1456-1465.

13. Grimme, S.; Antony, J.; Ehrlich, S.; Krieg, H., A Consistent and Accurate Ab Initio Parametrization of Density Functional Dispersion Correction (DFT-D) for the 94 Elements H-Pu. *The J. Chem. Phys.* **2010,** *132* (15), 154104.

14. Liechtenstein, A. I.; Anisimov, V. I.; Zaanen, J., Density-Functional Theory and Strong Interactions: Orbital Ordering in Mott-Hubbard Insulators. *Phys. Rev. B* **1995,** *52* (8), R5467-R5470.

15. Dudarev, S. L.; Botton, G. A.; Savrasov, S. Y.; Humphreys, C. J.; Sutton, A. P., Electron-Energy-Loss Spectra and the Structural Stability of Nickel Oxide: An LSDA+U study. *Phys. Rev. B* **1998,** *57* (3), 1505-1509.

16. Heyd, J.; Scuseria, G. E.; Ernzerhof, M., Hybrid Functionals Based on a Screened Coulomb Potential. *J. Chem. Phys.* **2003,** *118* (18), 8207-8215.

17. Krukau, A. V.; Vydrov, O. A.; Izmaylov, A. F.; Scuseria, G. E., Influence of the Exchange Screening Parameter on the Performance of Screened Hybrid Functionals. *J. Chem. Phys.* **2006,** *125* (22), 224106.